Hindawi
International Journal of Energy Research
Volume 2024, Article ID 6680018, 14 pages
https://doi.org/10.1155/2024/6680018

Research Article

Effects of Mechanical and Electrical Topologies on Piezoelectric Stacked Energy Harvesting in Vehicle Suspensions

Yang Li,[1,2] **Ruoyu Wang**,[1] **Zhao Wan**,[1] **Ming Chen**,[1,2] **and Guijie Liang**[3]

[1]*School of Automotive and Traffic Engineering, Hubei University of Arts and Science, 441000 Xiangyang, Hubei, China*
[2]*Hubei Key Laboratory of Power System Design and Test for Electrical Vehicle, 441000 Xiangyang, Hubei, China*
[3]*School of Physics and Electronic Engineering, Hubei University of Arts and Science, 441000 Xiangyang, Hubei, China*

Correspondence should be addressed to Yang Li; ruoxian0119@163.com

Received 31 July 2023; Revised 6 April 2024; Accepted 8 April 2024; Published 26 April 2024

Academic Editor: Jing Shi

The choice of mechanical and electrical topologies can affect piezoelectric energy harvesting efficiency, but the problem of achieving high-efficiency energy conversion in energy harvesters stacked as cantilevers has not been perfectly solved. This study focuses on the topology of piezoelectric elements in a stacked vehicle suspension vibration energy harvesting device. Through theoretical analysis, the stress expressions of the excited and driven elements are derived. The stress of the piezoelectric elements is affected by the positions of the connection and excitation points. A stress model was established for a four-piece piezoelectric element connected by a thin light rod in ANASYS. The simulation results show that the average stress in the piezoelectric bending element model is maximum when the excitation and connection points are located at both ends of the free end. Compared with the middle position of the free end of the piezoelectric element, the average stress of the model is increased by 92.904%. Considering the difference in voltage generated by piezoelectric elements, four kinds of electrical topology are designed and analyzed experimentally. When the driven elements are connected in parallel and then connected in series with the excited element, the output power varied the least with the change of load resistance. The system produces a high power and offers a wide selection of load resistors. When the load is 26 kΩ, a single set of four piezoelectric elements produces 86.407 mW of output power.

1. Introduction

Many countries are developing electric vehicle-related technologies and providing supportive policies [1]. To solve the problems of the short driving range and low energy recovery efficiency of electric vehicles, a number of energy recovery technologies have been proposed [2]. In the energy recovery and utilization of traditional vehicles, energy harvesting methods are mainly studied from three aspects: waste heat [3], braking energy [4], and vibration energy [5]. Vibration energy recovery technology has great application potential in both fuel and electric vehicles. Realizing the recovery and reuse of vehicle vibration energy is a problem worth addressing.

Vibration energy harvesters have been widely researched. Currently, these technologies mainly use principles such as electromagnetic [6], triboelectric [7], piezoelectric [8], and electrostatic [9] effects to function. To apply vibration energy harvesting technology to automobiles, researchers have integrated vibration energy harvesters with suspension systems, designing a new type of suspension with energy harvesting effects, such as hydraulic, electromagnetic, and piezoelectric suspension. The emergence of energy harvesting suspensions allows the substantial energy lost in suspension systems to be utilized [10–12]. Nazemian and Masih-Tehrani [13] proposed an active interconnected air suspension system that reduces energy consumption by utilizing external air pressure. Fu et al. [14] reviewed and investigated the structural forms, optimization methods, and control strategies of electromagnetic energy harvesting suspensions and prospected them. Guo et al. [15] proposed a hydraulic-integrated interconnected regenerative suspension and demonstrated that

this system could collect vibration energy while improving vehicle dynamics. Studies have also been conducted on energy harvesting in suspensions using the piezoelectric technology. Some of them use only piezoelectric technology for energy recovery, whereas others use hybrid piezoelectric-electromagnetic technology [16]. Piezoelectric energy harvesting technology has the advantages of low cost, high power density, good scalability, and great application potential in suspension systems [17–19]. The piezoelectric energy harvester installed in the suspension system can effectively recover the vibration energy dissipated in the suspension. To improve the recovery efficiency of piezoelectric suspension, various types of piezoelectric energy harvesters have been designed [20–22].

Significant progress has been made in the study of piezoelectric energy harvesting suspension. However, the issue of low energy conversion efficiency remains unresolved [23]. To enhance the efficiency of piezoelectric energy harvesting, some studies have focused on changing the size [24, 25], structure [26], material composition [27], and poling conditions [28] of piezoelectric materials to improve their recovery efficiency. Additionally, connecting multiple piezoelectric cantilever beams can increase the efficiency of piezoelectric harvesting. This is a common method for connecting piezoelectric bending elements to springs. Through theoretical analysis and experiments, the use of a spring has been shown to increase the system bandwidth and output power [29–31]. Although the effect of springs on the system has been studied, the connection position of the spring has not been considered. Researchers have also used other methods to connect piezoelectric cantilever beams. Hu et al. [32] designed a two-degree-of-freedom galloping-based piezoelectric energy harvester by mounting a secondary beam on a primary piezoelectric piece. Qin et al. [33] used an origami paper to connect two piezoelectric cantilever beams. These techniques effectively improved the bandwidth of the harvester and increased power generation. In these studies, although the connection mode between the piezoelectric pieces was considered, the influence of the mechanical topology on the output power was ignored.

Some studies used an electrical topology to improve energy harvesting efficiency. Khalili et al. [34] connected stacked piezoelectric elements in parallel to harvest mechanical energy from roads. However, there is a lack of discussion on connection methods such as series and hybrid connections. Niasar et al. [35] used three harvesting circuits to study the recovery efficiency of the proposed piezoelectric harvester and determined the optimal collection circuit. Cao et al. [36] studied the electrical connections between piezoelectric pieces. The results showed that the optimal resistance was affected by the series or parallel connections between the piezoelectric pieces. The influence of the number of piezoelectric elements on the optimal resistance was different for the different connection modes.

In our previous research, a stacked piezoelectric energy harvester was designed, and the influence of excitation mode and pavement grade on the energy conversion efficiency was studied [37, 38]. The method of three-order excitation and double-gear switching was proposed to harvest more electric energy. In this study, the mechanical and electrical topologies between piezoelectric elements in a device were studied. For the mechanical topology, the positions of the connections and excitation points between cantilever beams were investigated. Due to it being difficult to show the stress distribution of the cantilever beam experimentally, ANASYS was used to observe the stress of the cantilever beam at different connection and excitation points. For the electrical topology, multiple piezoelectric cantilever beams were connected using different circuits. Load was connected at the output end, and voltage was measured at both ends of the load. Based on the experimental data, the influences of the load and connection mode on the output power were analyzed to determine the best electrical topology mode.

2. Mechanical Topology

2.1. The Energy Harvesting Device. The energy harvesting device generated electric power by using vehicle vibrations as an excitation source, transmitting the vibrational energy to the excitation gear through a gear-rack structure. As the excitation gear rotates, it impacts the piezoelectric elements which are arranged in the form of cantilever beams. The application scenario of the energy harvesting device is shown in Figure 1.

A stacked piezoelectric bending element structure is carefully designed to enhance the output power and optimize the spatial utilization efficiency of the mechanical structure. It involves arranging the piezoelectric bending elements in a stacked manner around the gear to achieve higher vibration energy harvesting power. In the arrangement of the stacked groups, thin light rods are used to connect the piezoelectric bending elements and eliminate the phase differences. This ensures that the voltages between the elements do not cancel each other. Owing to the torsional deformation generated by contact with the excitation gear, some space is left between adjacent piezoelectric bending elements to prevent the obstruction of excitation. For piezoelectric bending elements that are not in direct contact with the gear, a synchronous bending action is induced by connecting thin light rods. Except for the wiring requirements, there is no need to leave significant space between them. As shown in Figure 2, four stacked structures are sequentially arranged around the excitation gear to maximize efficiency when utilizing the mechanical structure space.

In this study, the piezoelectric bending elements that are directly affected by the excitation gear are referred to as the "excited elements," and the other bending elements as the "driven elements." Each bending element comprises two layers of piezoelectric crystals and an intermediate copper substrate. A single-group stacked structure is shown in Figure 3.

During the bending process under force, piezoelectric bending elements convert the external impact energy into stored elastic potential energy. After the external excitation disappears, the piezoelectric bending elements release the stored energy. Part of this energy is dissipated as internal energy, and the rest is converted into electrical energy and

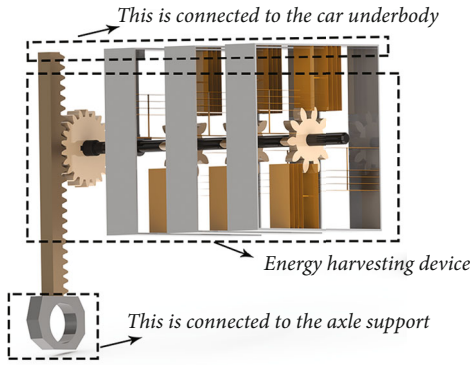

Figure 1: Application scenarios of energy harvester.

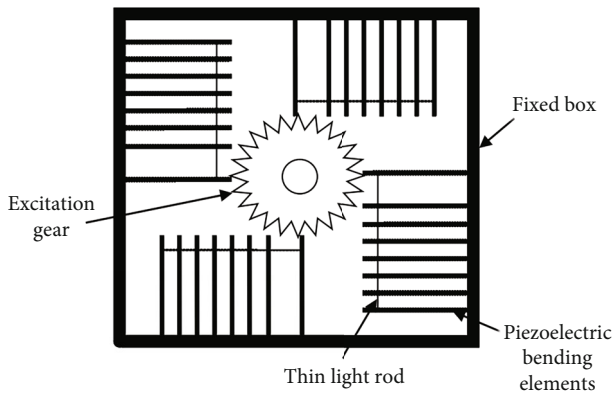

Figure 2: Energy harvesting device. The device consists of four sets of stacked piezoelectric bending elements and a gear. Gear is used instead of mass blocks to achieve excitation.

stored. The constitutive equation [39] for piezoelectric energy harvesting is as follows:

$$D_i = d_{ij}T_j + \varepsilon_{ik}^T E_k, \tag{1}$$

where D_i is the electric displacement, d_{ij} is the piezoelectric strain constant, T_j is the stress, ε_{ik}^T is the dielectric constant, and E_k is the electric field strength. The subscripts i, j, and k denote different directions in the material coordinate system.

2.2. Model Stress Analysis. During the energy storage process, the excited and driven elements experience different forces. It is assumed that both the excitation and connection points are positioned along the axis of the piezoelectric bending element. The force analysis of the excited and driven elements is shown in Figure 4.

After the excitation force F is applied to the excited element, the thin light rod generates a force F_r in the opposite direction. Moreover, the model is composed of $N+1$ bending elements that are connected in series by one thin light rod, which increases the bending section modulus of each bending element in the x-direction. The stress generated in the piezoelectric crystal of the excited element by bending can be expressed as follows:

$$\begin{aligned}\sigma_{E1} &= \frac{\int_0^{l_p}[F(l_m - x) - F_r(l_m - x_r - x)]dx}{(N+1)W_x l_p} \\ &= \frac{1}{(N+1)W_x}\left[\frac{l_p}{2}(F_r - F) + l_m(F - F_r) + F_r x_r\right].\end{aligned} \tag{2}$$

Throughout the motion process, the driven element is affected only by force F_r generated by the thin light rod. The average stress generated by the piezoelectric crystal in the driven element is given by

$$\sigma_{D1} = \frac{\int_0^{l_p} F_r(l_m - x_r - x)dx}{N(N+1)W_x l_p} = \frac{1}{N(N+1)W_x}\left[-\frac{F_r l_p}{2} + F_r(l_m - x_r)\right]. \tag{3}$$

Comparing Equations (2) and (3), although the expressions for stress are different between the excited and driven elements, the same deformations are generated when they are connected through a thin light rod. Therefore, the average stresses generated can be considered approximately equal. The relationship between F and F_r is derived as follows:

$$F_r = \frac{(2l_m - l_p)N}{(2l_m - l_p - 2x_r)(1+N)}F. \tag{4}$$

When either the excitation point or the connection point is not located on the central axis, the excitation force F acting on the bending element not only causes bending in the x -direction but also induces bending and twisting in the y -direction (Figure 5). In this case, the stress generated in the excited element comprises two normal stress components and one shear force. The difference in the positions of the connection and excitation points results in different degrees of deformation, thereby affecting the open-circuit voltage generated by the energy harvester.

For the driven elements, the thin light rod exerted a force to induce twisting. The stiffness of the piezoelectric bending element is improved when the thin light rod is applied. This resulted in the minimal impact of the force on the driven elements. As a result, the torsion from driven elements can be ignored. Therefore, the difference in the stress generation between the excited and driven elements primarily reflects the shear force and normal stress in the y-direction. The stress induced by bending in the x-direction is analyzed in the previous section. The normal and shear stresses owing to bending in the y-direction can be expressed as follows:

$$\begin{aligned}\sigma_{E2} &= \frac{\int_0^w F(s-y) - F_r y dy}{(N+1)wW_y} = \frac{2Fs - Fw - F_r w}{2(N+1)W_y}, \\ \tau_E &= \frac{(F - F_r)s}{2(N+1)W_t}.\end{aligned} \tag{5}$$

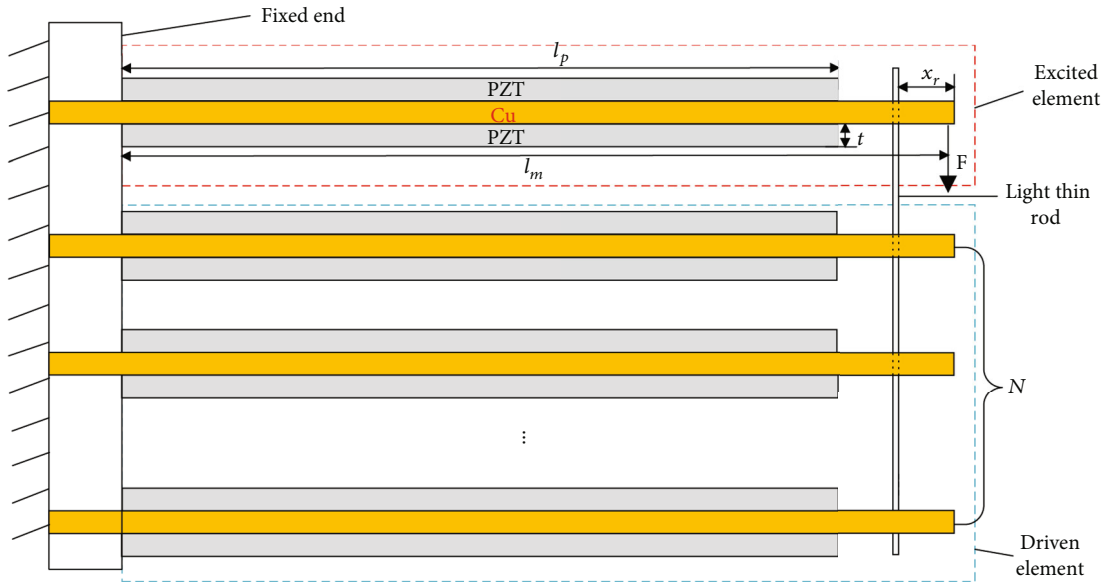

Figure 3: Stacked piezoelectric bending element structure. Each structure comprises an excited element, N-driven elements, and a thin light rod. The rod allows simultaneous bending between bending elements.

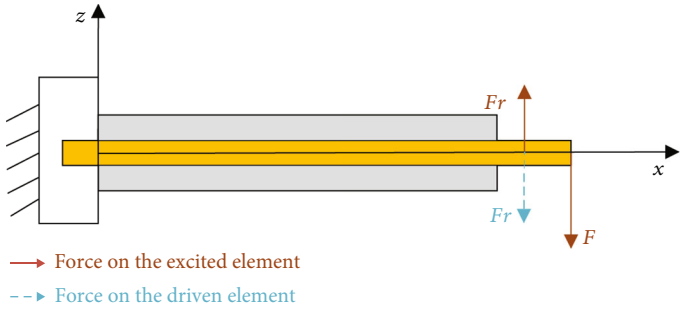

Figure 4: Force analysis of the excited and driven elements along the x-axis.

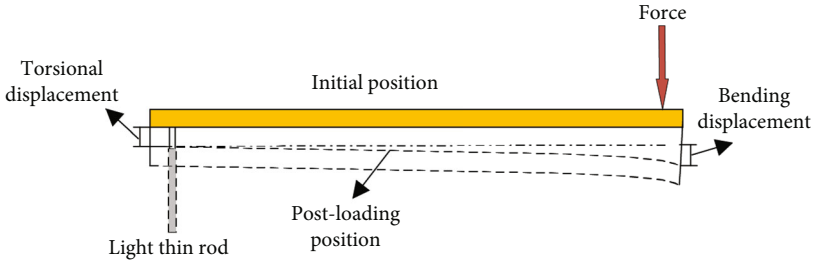

Figure 5: Bending situation of the excited element at a noncentral axis position.

By combining Equations (3)–(5), the relationship between the number of driven elements N and stress multiplication factor n_F for the excited and driven elements is as follows:

$$n_F = \frac{\left[2sW_t\left(2l_m - l_p - 2x_r\right)(1+N) + \left(2l_m - l_p - 2x_r - 2x_rN\right)\left(sW_y - wW_t\right)\right]W_x}{\left(2l_m - l_p - 2x_r\right)\left(2l_m - l_p\right)W_yW_t} + 1. \tag{6}$$

In Equation (6), the shape of a single bending element is fixed. It is clear that the stress multiplicative factor is affected by the distance x_r from the connection point to the free end, vertical distance s between the two forces, and number of driven elements N. In addition, s and x_r are subject to changes in the mechanical topology.

As s increases, the excited element generates more torsion, which in turn increases the resulting stress. As x_r

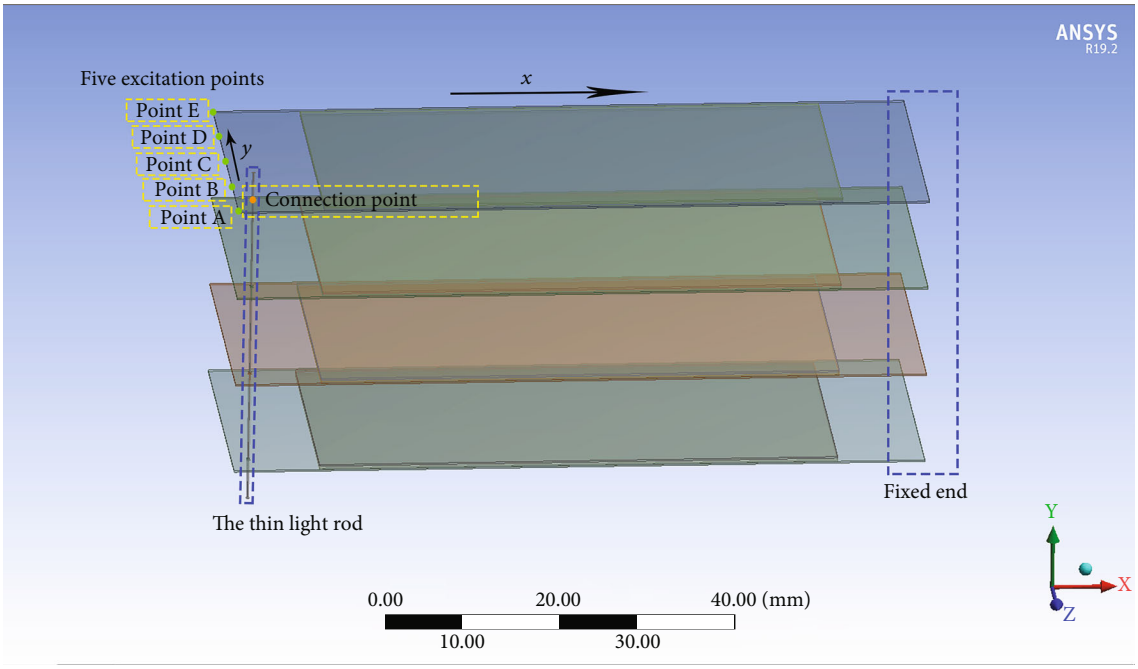

Figure 6: Simulation model.

decreases, the connection point gradually moves toward the end of the cantilever beam, causing the larger cantilever to bend. Therefore, the greater the distance between the connection and excitation points and the closer the connection point is to the free end of the cantilever beam, the greater the n_F. The parameter x_r can be approximated as 0, and Equation (6) can be simplified.

$$n_F = \frac{\left[2sW_t(1+N) + \left(sW_y - wW_t\right)\right]W_x}{\left(2l_m - l_p\right)W_y W_t} + 1. \tag{7}$$

3. Electrical Topology

In the previous section, we determined the mechanical topology and analyzed stress generation within the bending elements of the group. The stress in the excited element under external excitation primarily consists of three components, and the generated voltage is primarily in the 3-directions. Therefore, the electrical displacements produced by the excited and driven elements in the 3-directions are as follows:

$$\begin{aligned} D_{E3} &= d_{31}(\sigma_{E1} + \sigma_{E2}) + \varepsilon_{33}E_{E3}, \\ D_{D3} &= d_{31}\sigma_{D1} + \varepsilon_{33}E_{D3}, \end{aligned} \tag{8}$$

where D_{E3} and D_{D3} are the electric displacement of the excited and driven elements in the 3-direction, respectively; E_{E3} and E_{D3} are the electric field strength of the excited and driven elements in the 3-direction, respectively; d_{31} is the piezoelectric strain constant; ε_{33} is the dielectric constant.

The dielectric properties of piezoelectric crystals follow the electrostatic law known as the dielectric relation, which allows for the conversion between electric displacement D_3 and electric field strength E_3. E_3 is also related to voltage V [40], thus yielding the expression relating electric displacement D_3 and voltage V:

$$D_3 = \frac{\varepsilon_{33}V}{r}, \tag{9}$$

where r is the thickness of the dielectric layer.

Based on the above expression, when the excited element bends and generates voltage, the presence of positive stresses in 2-directions leads to differences in voltage between the excited and driven elements. Therefore, the voltage multiplication factor n_V between the excited and driven elements can be expressed as

$$n_V = 1 + \frac{[2s(1+N) - w(1+2N)]W_x}{W_y\left(2l_m - l_p\right)}. \tag{10}$$

The connected harvesting device can be considered an equivalent circuit model with an open-circuit voltage U_t and internal capacitance C_t. When connected to a load resistor R, the output power generated is as follows:

$$P = \frac{\omega^2 R U_t^2}{2\omega^2 R^2 + \left(2/C_t^2\right)}. \tag{11}$$

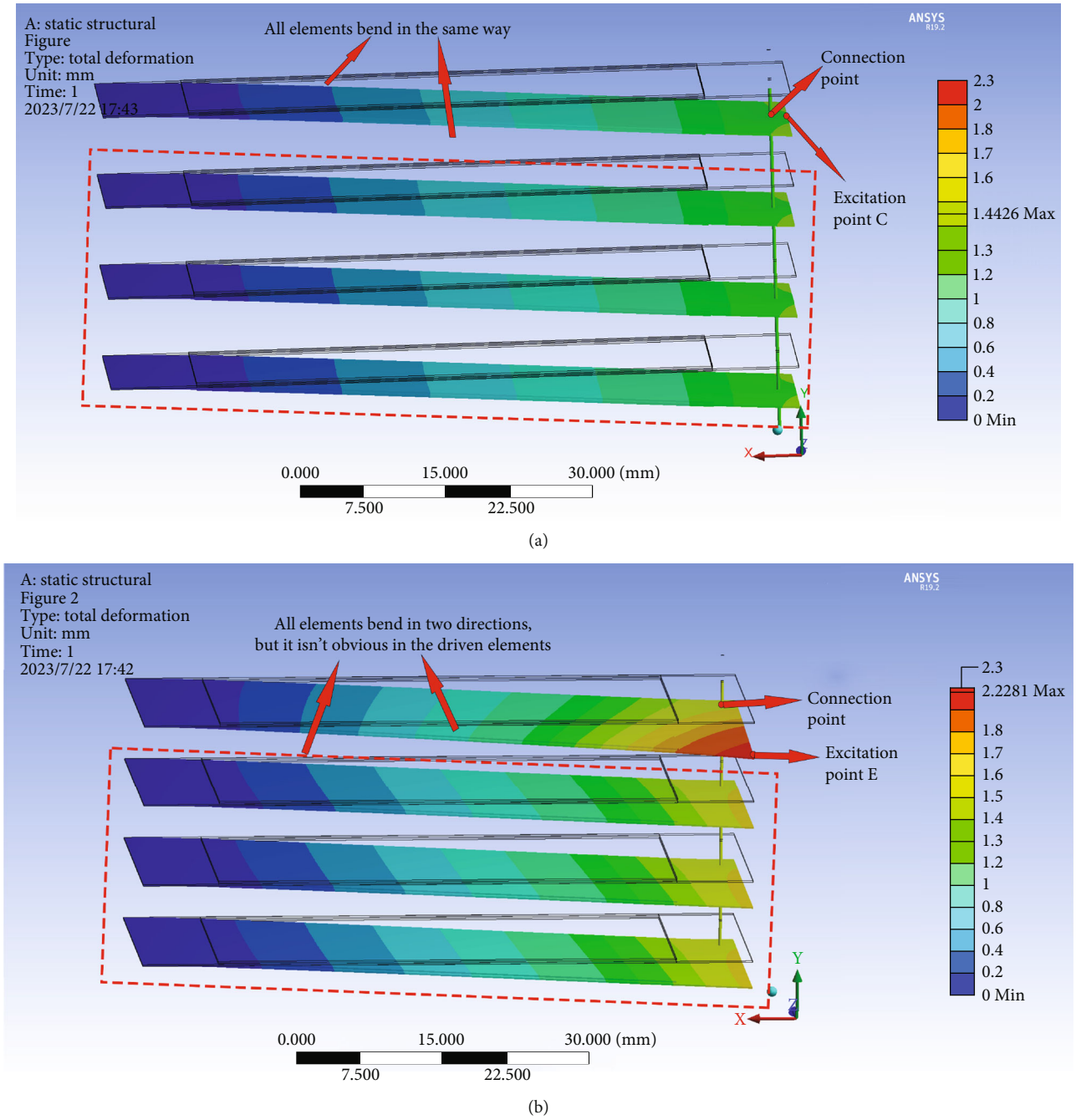

Figure 7: Model displacement. (a) Connection point and excitation point both at C. (b) Connection point at A and excitation point at E.

U_t and C_t are positively correlated with the output power P. As the electrical topology of the piezoelectric bending elements within a device can influence U_t and C_t, it is necessary to study the electrical topology to maximize the output power.

Owing to the connection of all the bending elements within each group through a thin light rod, the resonant frequencies of the excited and driven elements are the same, indicating that their impedances are equal. Let the open-circuit voltage generated by each driven element be U. Then, the open-circuit voltage generated by the excited element is $n_V U$, and the internal capacitance is denoted as C for all elements within each group. Each group of models consisted of $N + 1$ piezoelectric bending elements. As shown in Figure 1, four groups of models are placed in a single energy harvesting device. Four different topology methods for the bending element are analyzed.

(a) Topology 1: when all piezoelectric bending elements are connected in series, the open-circuit voltage and

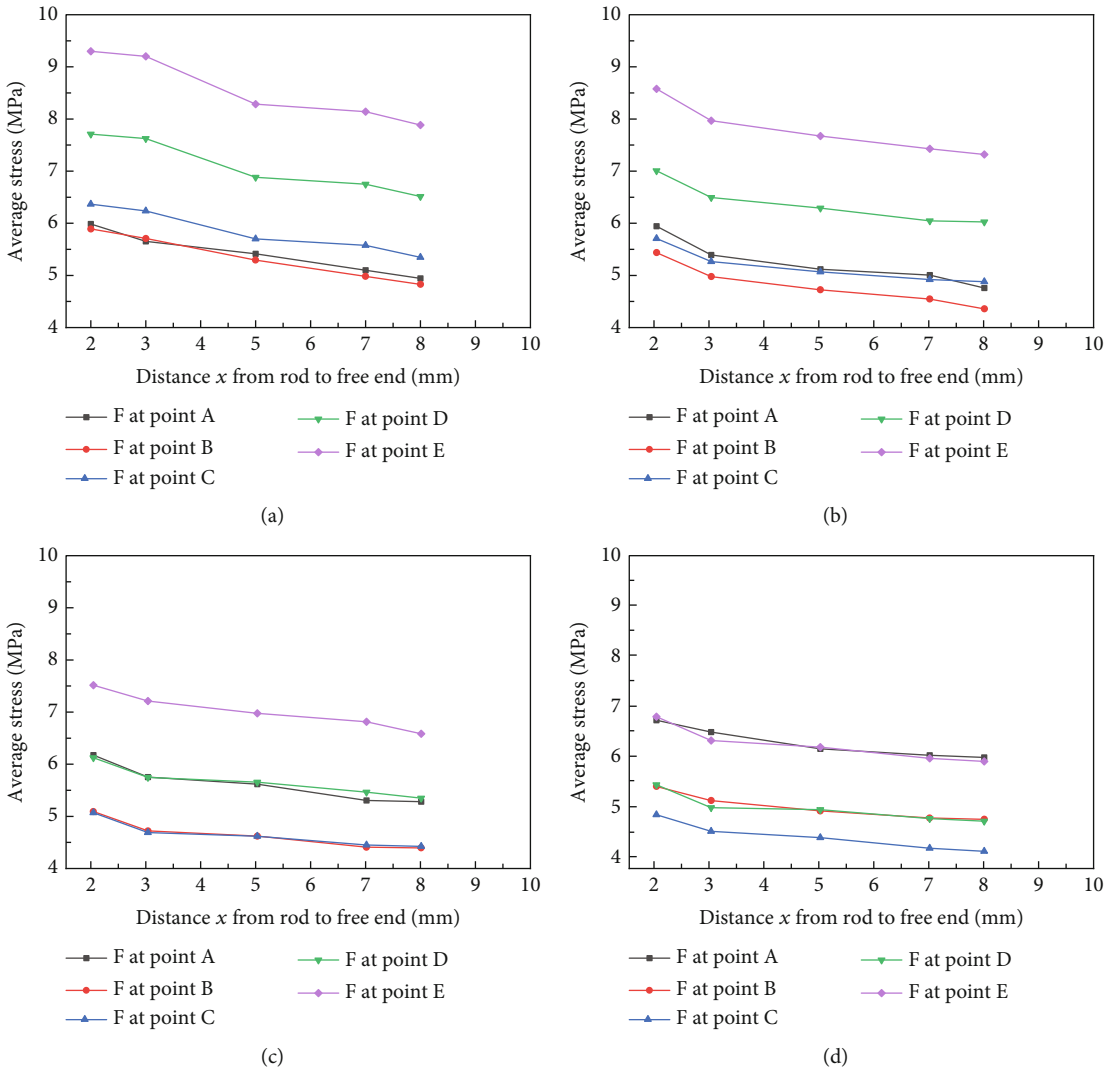

Figure 8: Plot of the average stress with respect to the position of the excitation point and the connection point. The positions of the connection point include x and y. (a) $y = 4$ mm. (b) $y = 8$ mm. (c) $y = 12$ mm. (d) $y = 16.5$ mm.

internal capacitance of the energy harvesting device can be expressed as follows:

$$U_{t1} = (n_V + N)U,$$
$$C_{t1} = \frac{C}{(N+1)}. \tag{12}$$

(b) Topology 2: the driven elements are connected in parallel. Subsequently, the parallel group of driven elements is connected in series with the excited element. The open-circuit voltage and internal capacitance of the energy harvesting device can be expressed as follows:

$$U_{t2} = (n_V + 1)U,$$
$$C_{t2} = \frac{NC}{N+1}. \tag{13}$$

(c) Topology 3: when all piezoelectric bending elements are connected in parallel, the open-circuit voltage and internal capacitance of each group of models can be expressed as follows:

$$U_{t3} = \frac{(n_V + N)U}{N+1},$$
$$C_{t3} = (N+1)C. \tag{14}$$

(d) Topology 4: the driven elements are connected in series. Subsequently, the series group of driven elements is connected in parallel with the excited element. The open-circuit voltage and internal capacitance of the energy harvesting device can be expressed as follows:

$$U_{t4} = \frac{(n_V + 1)NU}{N+1},$$
$$C_{t4} = \frac{N+1}{N}C. \tag{15}$$

By substituting Equations (12)–(15) into equation (11) individually, it can be observed that during the variation in the load resistance, there is a resistance value for each connection mode that maximizes the output power. Therefore, the electrical topology must be selected in conjunction with the load resistance. Hence, experimental investigations are necessary to determine the optimal electrical topology based on actual energy harvesting conditions.

4. Simulation and Experiment

4.1. Simulation Model Establishment and Result Analysis. According to the piezoelectric energy harvesting constitutive equation, the voltage generated by the piezoelectric bending element is positively correlated with the induced stress. Therefore, the generated voltage can be predicted by studying the stress.

In this study, a set of stacked structures with four piezoelectric bending elements is used as an example. The effects of different mechanical topologies on the stress generated by the excited and driven elements under external excitation are studied. Each bending element is configured with a three-layer structure (PZT-Cu-PZT), with tight fixation between layers to ensure model stability under external forces. After creating four identical piezoelectric bending elements, a thin light rod is inserted into the substrate to connect the layers. The rod is made of a material with high stiffness to prevent excessive deformation when subjected to external forces. To simulate the effect of forces on the side of the substrate, point loads are applied as force points at five locations spaced 12 mm apart. During the simulation, one side of the model connected to the rod served as the free end, whereas the other side is fixed using a fixed support boundary condition. The simulation model is shown in Figure 6.

As shown in Figure 6, points A, B, C, D, and E are designated as the locations of the external excitation. The radius of the rod is 1 mm, and its center is positioned along the x -axis within the range of 1–9 mm, and along the y-axis within the range of 0–33 mm. Because of the symmetric structure of the bending element along the central axis, the variation of the center position along the y-axis in the simulation ranges from 0 to 16.5 mm.

In Section 2.2, the effects of the insertion and excitation points on the central axis are discussed in terms of the bending form of the piezoelectric bending element. The displacement of the piezoelectric bending elements in the model by conducting simulations is observed. Figure 7(a) shows the result when both the connection and excitation points are located at point C, and Figure 7(b) shows the result when the connection and excitation points are located at point A and point E, respectively.

As shown in Figure 7(a), when both the connection and excitation points are located on the central axis, the displacement generated by each piezoelectric bending element is uniformly distributed. As shown in Figure 7(b), when the connection and excitation points are not on the central axis, the displacement of the excited element exhibits a significant attenuation trend from the force application point toward the outer region. However, the displacement of the driven elements tended to be more uniformly distributed. The average displacements of both elements are greater than what is observed in Figure 7(a). Therefore, the positions of the excitation and connection points result in significant differences in the degree of bending.

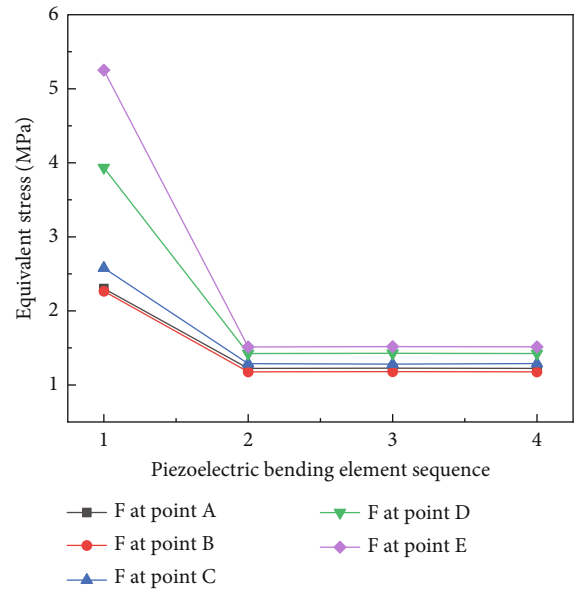

Figure 9: Average stress difference of each bending element in the group at different excitation positions.

To determine the mechanical topology, the positions of the excitation points are fixed, and the variation in the stress magnitude to the change in the connection point is obtained by longitudinally or laterally moving the position of the thin light rod. In addition, with the position of the rod fixed, the same external force is applied at different positions on the bending elements, and the stress magnitude of each piezoelectric bending element at different excitation point positions is determined. The mechanical topology is determined when the maximum stress is achieved. The average stresses generated by the model at different excitation and connection point positions are shown in Figure 8.

When the excitation point is at point E, the model generates a higher stress. By analyzing the data of curve F at point E, when the rod was moved along the x-axis, the total stress decreased by 35.625, 30.718, 17.844, and 1.043%. A larger stress was generated when $x = 2$ mm. By comparing the data at $x = 2$ mm in the stress curves for F at point E in the four groups, it is evident that as the rod moved along the y-axis from 4 to 16.5 mm, the total stress in the model gradually decreased by 27.098%, from 9.298 MPa to 6.779 MPa. Therefore, when the center coordinates of the light thin rod are $x = 2$ mm and $y = 4$ mm, and the excitation point is at point E, the model generates the highest total stress.

After determining the mechanical topology, the stress variations in each piezoelectric bending element within the model are analyzed. This analysis facilitates the subsequent

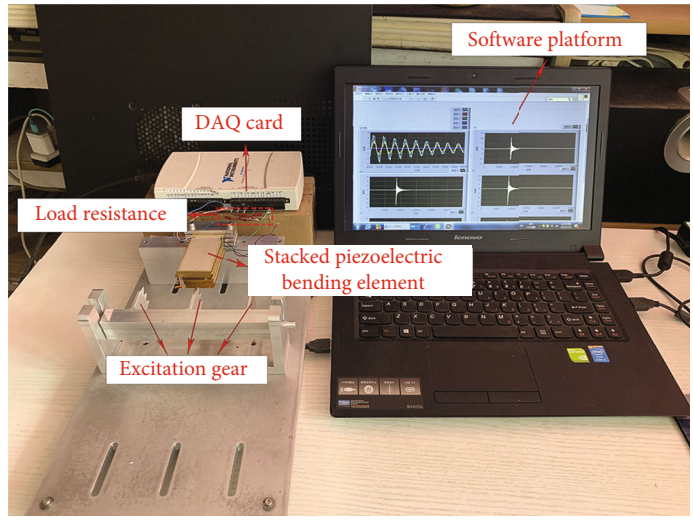

Figure 10: Experimental platform for energy harvesting mechanism.

Table 1: Parameters of a piezoelectric bending element and gear pitch.

Quality factor, Q_m	70
Electromechanical coupling factor, K_p	0.65
Piezoelectric constant, D_{31} 10^{-12} (C/N)	-186
Piezoelectric constant, D_{33} 10^{-12} (C/N)	670
Piezoelectric constant, D_{15} 10^{-12} (C/N)	660
Dielectric constant, $\varepsilon_{11}/\varepsilon_0$	3130
Dielectric constant, $\varepsilon_{33}/\varepsilon_0$	3400
Size of piezoelectric ceramic (mm)	$60 \times 31 \times 0.2$
Size of base plate (mm)	$80 \times 33 \times 0.2$
Gear pitch (mm)	7

study of the electrical topology. The same excitation is applied at five loading points to obtain the magnitude of the stress generated in each piezoelectric bending element, as shown in Figure 9.

Based on the stress results shown in Figure 9, the excited elements generated significantly higher stress than the driven elements. With a change in the excitation point, the average stress generated by the excited element increased by 128.104%, and that of the driven elements increased by 23.654%. The average stress difference between the driven elements is approximately 0.3%. Therefore, during energy harvesting, it is feasible to consider a unified recovery approach for the driven elements. To achieve maximum power recovery, it is essential to consider the electrical topology of the bending elements. This approach allows the electrical energy generated by the excited and driven elements to be harvested maximally.

4.2. Experimental Testing and Result Analysis. The experimental platform for measuring the energy harvesting mechanism is illustrated in Figure 10. To evaluate the output voltage, piezoelectric bending elements are connected to a load resistor. In the experiment, the piezoelectric bending elements are fixed, and gears are used for excitation. The parameters of a single piezoelectric bending element are shown in Table 1. The output end of the piezoelectric bending elements is connected to a load resistor for voltage division, and data are collected using a DAQ card. The collected data are transferred to LabVIEW for analysis. During the excitation, the DAQ card captures the voltage signal across the load resistor. Owing to the DAQ card having a voltage range of -10 V to 10 V, a resistor is utilized for voltage division in the test of the optimal load resistance. By collecting the voltage data from the divider resistor, the output voltage of the bending element model can be obtained by multiplying it by the corresponding factor.

To assess the voltage disparity between the excited and driven elements in the model, the voltages generated by all four piezoelectric bending elements are measured simultaneously.

When the excitation and connection points are in the middle position of the piezoelectric elements, the voltage curves produced by the four bending elements are shown in Figure 11.

The peak-to-peak voltage U_p in the first period is compared for each dataset. The U_p generated by the excited element is 7.837 V. The U_p generated by the three driven elements are 3.238, 3.184, and 3.101 V, respectively. The voltage generated by the excited element is higher than that generated by the driven element, and the voltages generated among the driven elements are almost the same. Analysis of the vibration process of the piezoelectric bending elements shows that the three driven elements are only affected by the rod, and the stress is almost the same. Thus, the generated voltages are nearly the same. Since the vibration frequencies of the excited and the driven elements are nearly identical, the equivalent impedance of the piezoelectric elements is regarded as the same.

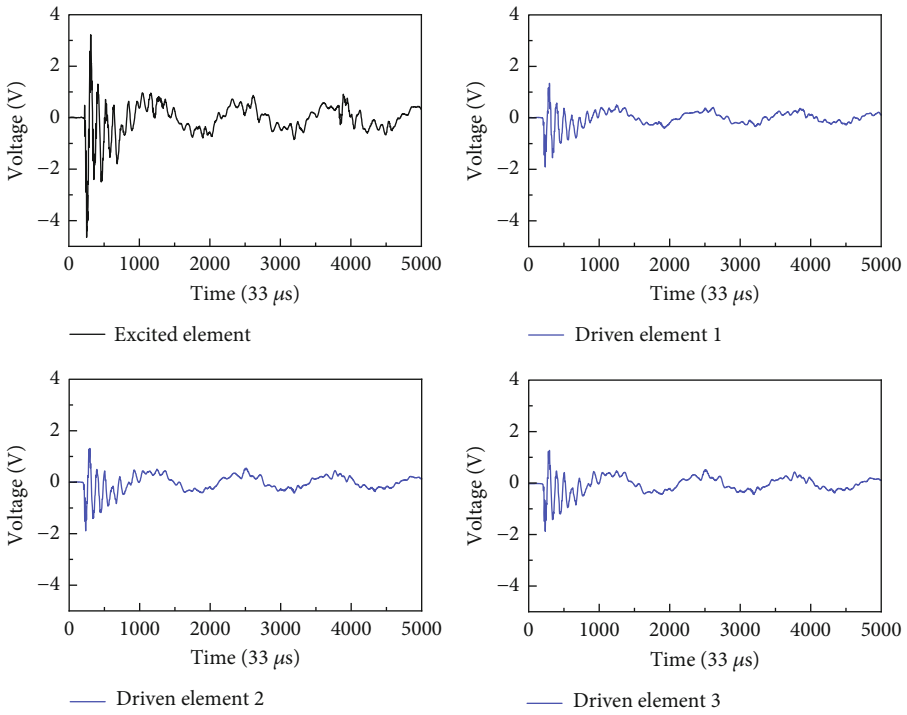

Figure 11: Voltage curves of the four elements in the model.

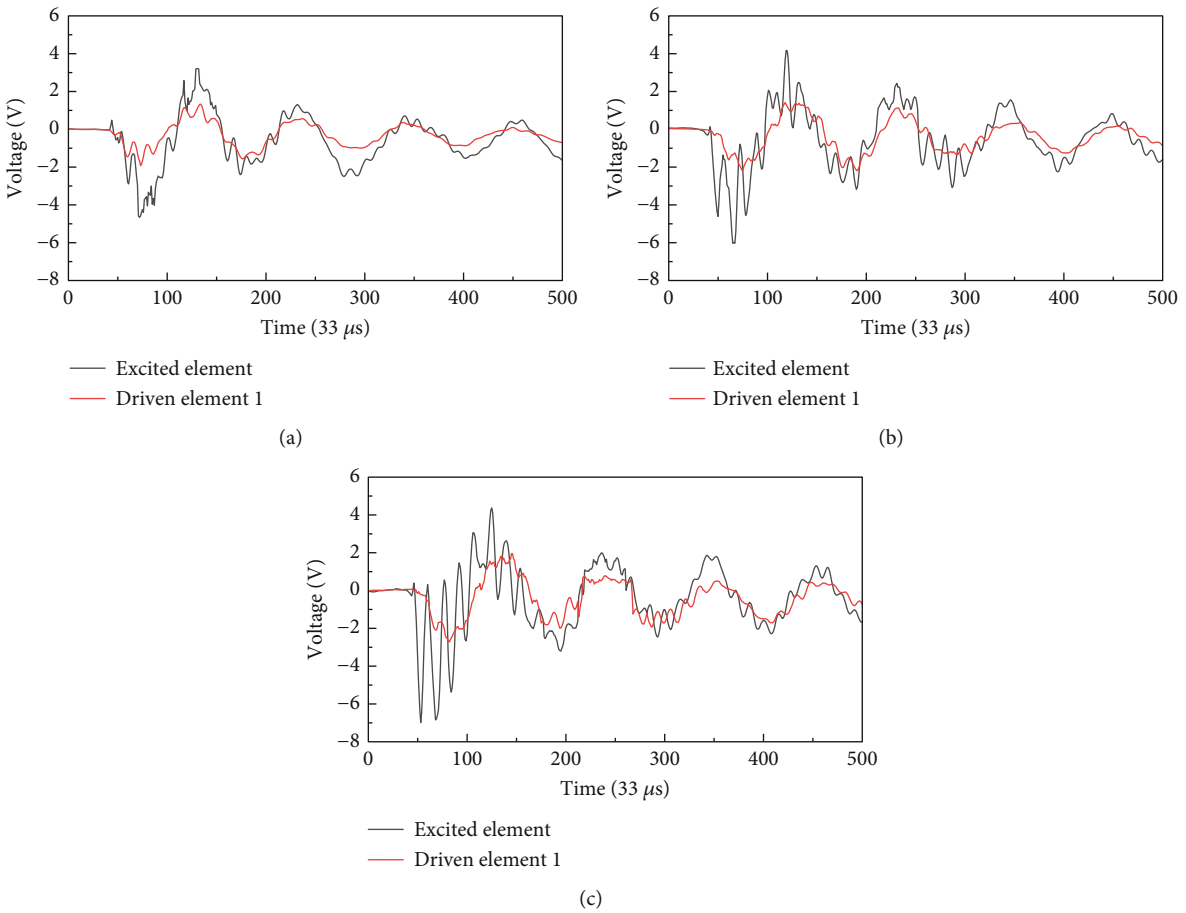

Figure 12: Voltage curves of the excited and driven elements at different excitation positions. (a) F at point C. (b) F at point B. (c) F at point A.

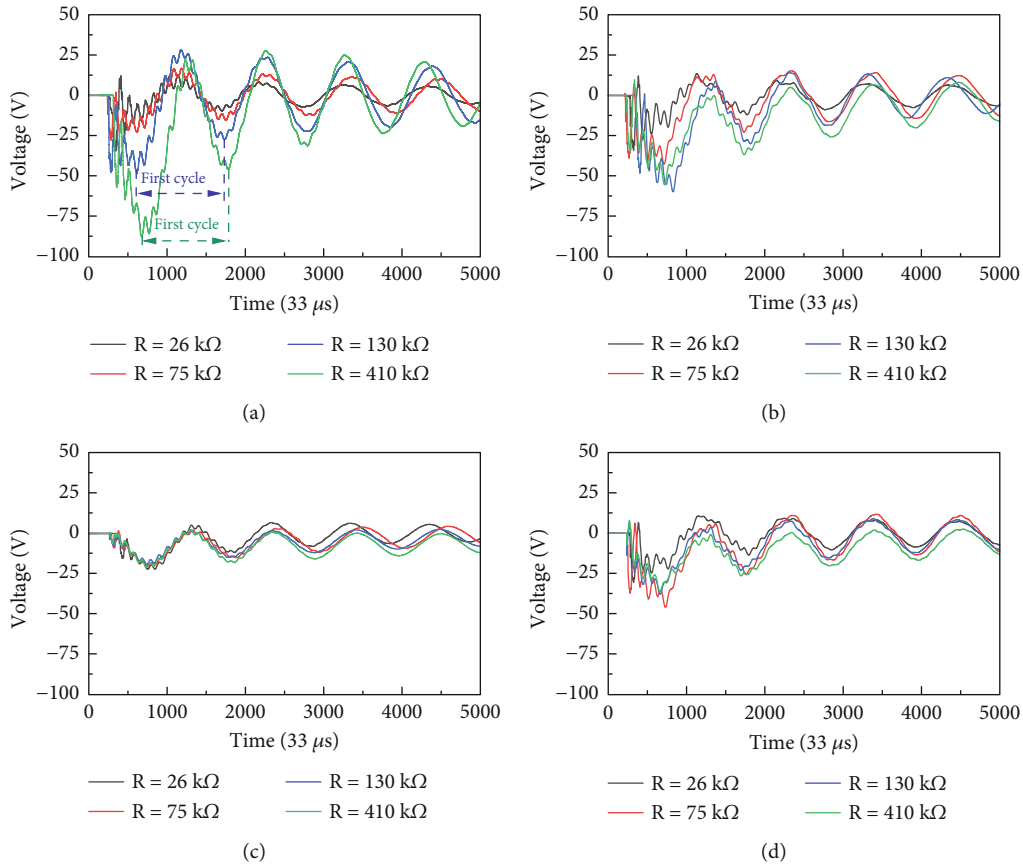

Figure 13: Aggregate output voltage under four different connection configurations. (a) Topology 1. (b) Topology 2. (c) Topology 3. (d) Topology 4.

Testing revealed that a single piezoelectric element has an equivalent resistance of approximately 100 kΩ. Based on this, the calculated equivalent resistances for the piezoelectric elements within the four topology configurations are 400 kΩ, 133 kΩ, 25 kΩ, and 75 kΩ, respectively. Appropriate resistance values will be selected in subsequent experiments to determine the maximum output power of each configuration.

In energy harvesting processes, the excitation gear impacts the bending elements multiple times in a short period. Therefore, this study only considers several initial small cycles of the vibration process for the bending elements. Voltage data for the excited and driven elements are collected from three sets of different excitation positions. The results are presented in Figure 12.

Based on the test data, the voltage phase difference between the excited element and the drive element in the energy harvester can be negligible in a large period. However, there is a significant difference in the voltage magnitude between the excited and driven elements during the initial vibration. By comparing the three graphs, it is evident that an increase in the vertical distance between the excitation and connection points results in higher voltages generated by both the excited and driven elements and a voltage difference for each small period in the voltage curve. The U_p of the first cycle is compared. Piezoelectricity generated by the excited element increases by 44.348%, and that by the driven element increases by 43.941%. Moreover, as the excitation point moves to the edge, the excited element produces lateral torsion, which increases the vibration frequency and output voltage of the excited element. This change reflects the direct relationship between the position of excitation and the dynamic response of the system.

To study the electrical topology, the four connection methods proposed in Section 3 are used to connect the piezoelectric bending elements under the optimized mechanical topology. In the experiment, four resistance values are selected to investigate the output voltage under each connection method as the resistance increases. The corresponding voltage curves are shown in Figure 13.

The U_p in the first cycle of each dataset is calculated (Table 2), and the U_p^2/R is obtained. The output power for each type of electrical topology is illustrated through the value of U_p^2/R.

The choice of electrical topology results in a difference in the internal resistance of the device. In the optimized mechanical topology, the vibration frequency of the excited element is increased, and the impedance is reduced. This modification alters the optimum load resistance of the device. From Table 2, the choice of resistance will affect the output power of the energy harvester. However, in practical application,

Table 2: Electrical topology experimental data.

Topology method (four piezoelectric elements)	Load resistance (kΩ)	Peak-to-peak voltage (V)	U_p^2/R (mW)
Topology 1	26	47.686	87.459
	75	44.128	25.964
	130	76.947	45.545
	410	110.166	29.601
Topology 2	26	47.398	86.407
	75	54.859	40.127
	130	68.341	35.927
	410	55.35	7.472
Topology 3	26	27.433	28.945
	75	22.204	6.574
	130	21.389	3.519
	410	23.657	1.365
Topology 4	26	40.301	62.468
	75	52.504	36.756
	130	39.905	12.249
	410	36.889	3.319

the output of the energy harvester is connected to an AC/DC circuit. By optimizing topology, the equivalent resistance of the AC/DC circuit can be adjusted. Comparing all values of U_p^2/R, topology 1 and topology 2 result in higher power compared to other topologies. However, as the load resistance increases, the power of topology 1 initially decreases significantly before increasing. The power of topology 2 exhibits a monotonic decrease with the increasing load resistance, with a reduction rate that is less than that of topology 1 and topology 3. For topology 4, the power remains lower than that of topology 2. Consider that the output of the energy harvester is connected to the AC/DC circuit. Although the equivalent resistance of the load can be adjusted by optimizing the topology of the back-end energy storage device of the AC/DC circuit, the equivalent resistance is not very accurate. The trend in the power variation suggests that the maximum power can be more readily obtained in topology 2, owing to its lower sensitivity to changes in load resistance. The power of topology 1 is almost equal to that of topology 2 and higher than that of topology 3 and topology 4 when the load resistance is 26 kΩ. However, when the load resistance is 75 kΩ, the power of topology 1 is only 25.964 mW, and the power of topology 2 is the highest. A comprehensive assessment led to the conclusion that topology 2 is the most suitable electrical topology.

5. Conclusions

The mechanical and electrical topologies of a stacked piezoelectric energy harvesting device are investigated, and simulation models and experimental platforms are designed. Regarding the mechanical topology, the theoretical expressions for the stress generated in excited and driven elements during bending are derived. A stress model was established for a four-piece piezoelectric element connected by a thin light rod in ANASYS. It is found that the average stress in the piezoelectric bending element model is maximum when the excitation and connection points are located at both ends of the free end. To verify the simulation results, test experiments are carried out. The peak-to-peak voltage U_p in the first period is compared for each dataset. When the position of the rod is fixed and the excitation point is moved from point C to point A, the U_p generated by the excited element increases by 44.348%, and that by the driven element increases by 43.941%.

Based on determining the mechanical topology, the electrical topology is analyzed. From the equivalent circuit power expression, it is evident that a larger open-circuit voltage and internal capacitance in the energy harvesting device result in a higher power. Considering the difference in voltage between piezoelectric elements, four different circuit configurations of bending elements are proposed, and the electrical topology is determined by experiments. The experimental results indicate that topology 1 and topology 2 achieve higher power than topologies 3 and 4. Topology 2 has higher output power and lower sensitivity to load resistance changes than topology 1. Therefore, topology 2 is the preferred electrical topology. When the load is 26 kΩ, a single set of four piezoelectric elements produces 86.407 mW of output power.

Nomenclature

l_m: The length of the substrate (mm)
l_p: The length of the piezoelectric crystal (mm)
w: The width of the piezoelectric crystal (mm)
W_x: The flexural section modulus of the bending element for the x-axis (mm^3)
W_y: The flexural section modulus of the bending element for the y-axis (mm^3)
W_t: The torsional section modulus of the bending element (mm^3)
F: External excitation (N)
F_r: Excitation applied to the driven elements (N)
x_r: Distance from the connecting rod to the free end (mm)
s: The vertical distance between F and F_r (mm)
N: The number of driven elements in a single-group model
n_F: The stress multiplication factor between the excited element and the driven elements
n_V: The voltage multiplication factor between the excited element and the driven elements
U: The open-circuit voltage of a single piezoelectric bending element (V)
C: The internal capacitance of a single piezoelectric bending element (F)

Data Availability

The simulation and experiment data used to support the findings of this study are available from the corresponding author upon request.

Conflicts of Interest

The authors declare that they have no conflicts of interest.

Acknowledgments

This research was supported by the Natural Science Foundation of Hubei Province (2022CFD084) and the Key Project of Hubei Provincial Department of Education (D20222602).

References

[1] Z. H. Li, A. Khajepour, and J. C. Song, "A comprehensive review of the key technologies for pure electric vehicles," *Energy*, vol. 182, pp. 824–839, 2019.

[2] S. X. Bai and C. H. Liu, "Overview of energy harvesting and emission reduction technologies in hybrid electric vehicles," *Renewable and Sustainable Energy Reviews*, vol. 147, article 111188, 2021.

[3] W. Sun, F. Y. Yi, D. H. Hu, and J. M. Zhou, "Research on matching design method of waste heat reuse system of fuel cell vehicle considering system energy consumption and waste heat exchange rate," *International Journal of Energy Research*, vol. 45, no. 4, pp. 5470–5485, 2021.

[4] B. Zhao, R. J. Liu, D. P. Shi, S. P. Li, Q. L. Cai, and W. C. Shen, "Optimal control strategy of path tracking and braking energy recovery for new energy vehicles," *Processes*, vol. 10, no. 7, p. 1292, 2022.

[5] D. D. Cao, X. Xu, W. S. Li, J. Hu, and Z. G. Kong, "Research on random vibration condition of driving motor system for new energy passenger vehicle," *Energy Reports*, vol. 8, pp. 988–996, 2022.

[6] J. Y. Zhang, Y. J. Zhi, K. Yang, N. Hu, Y. Peng, and B. Wang, "Internal resonance characteristics of a bistable electromagnetic energy harvester for performance enhancement," *Mechanical Systems and Signal Processing*, vol. 209, article 111136, 2024.

[7] X. H. Wang, G. F. Yin, T. Sun, X. J. Xu, G. Rasool, and K. Abbas, "Mechanical vibration energy harvesting and vibration monitoring based on triboelectric nanogenerators," *Energy Technology*, vol. 12, no. 4, 2024.

[8] Z. Y. Xiang, J. K. Zhang, S. J. Li et al., "Friction-induced vibration energy harvesting via a piezoelectric cantilever vibration energy collector," *Tribology International*, vol. 189, article 108933, 2023.

[9] M. Pourahmadi-Nakhli, B. Sasanpour, M. Mahdavi, and M. Sharifpur, "Optimal heartbeat energy harvesting using electrostatic energy harvesters," *Energy Technology*, vol. 11, no. 11, 2023.

[10] A. Ali, A. Ahmed, M. Ali et al., "A review of energy harvesting from regenerative shock absorber from 2000 to 2021: advancements, emerging applications, and technical challenges," *Environmental Science and Pollution Research*, vol. 30, no. 3, pp. 5371–5406, 2023.

[11] X. Y. Lv, Y. J. Ji, H. Y. Zhao, J. B. Zhang, G. Y. Zhang, and L. Zhang, "Research review of a vehicle energy-regenerative suspension system," *Energies*, vol. 13, no. 2, p. 441, 2020.

[12] M. A. A. Abdelkareem, L. Xu, M. K. A. Ali et al., "Vibration energy harvesting in automotive suspension system: a detailed review," *Applied Energy*, vol. 229, pp. 672–699, 2018.

[13] H. Nazemian and M. Masih-Tehrani, "Development of an optimized game controller for energy saving in a novel interconnected air suspension system," *Proceedings of the Institution of Mechanical Engineers Part C-Journal of Mechanical Engineering Science*, vol. 234, no. 13, pp. 3068–3080, 2020.

[14] C. Z. Fu, J. Y. Lu, W. Q. Ge, C. Tan, and B. Li, "A review of electromagnetic energy regenerative suspension system & key technologies," *Cmes-Computer Modeling in Engineering & Sciences*, vol. 135, no. 3, pp. 1779–1824, 2022.

[15] S. J. Guo, L. Chen, X. K. Wang, J. Y. Zhou, and S. B. Hu, "Hydraulic integrated interconnected regenerative suspension: modeling and characteristics analysis," *Micromachines*, vol. 12, no. 7, p. 733, 2021.

[16] M. Iqbal, M. M. Nauman, F. U. Khan et al., "Vibration-based piezoelectric, electromagnetic, and hybrid energy harvesters for microsystems applications: a contributed review," *International Journal of Energy Research*, vol. 45, no. 1, pp. 65–102, 2021.

[17] Y. L. A. Morangueira and J. C. D. Pereira, "Energy harvesting assessment with a coupled full car and piezoelectric model," *Energy*, vol. 210, article 118668, 2021.

[18] C. Covaci and A. Gontean, "Piezoelectric energy harvesting solutions: a review," *Sensors*, vol. 20, no. 12, p. 3512, 2020.

[19] J. Siang, M. H. Lim, and M. S. Leong, "Review of vibration-based energy harvesting technology: mechanism and architectural approach," *International Journal of Energy Research*, vol. 45, no. 5, pp. 1866–1893, 2018.

[20] C. Li, D. Hong, K. H. Kwon, and J. Jeong, "Enhancement of energy harvesting performance for a piezoelectric cantilever using a spring mass suspension," *Journal Of Vibroengineering*, vol. 16, no. 1, pp. 116–125, 2014.

[21] Y. L. Wang, T. L. Wu, Z. H. Ran, B. Z. Lv, and S. Wang, "Modeling analysis and experiments of a novel hydro-pneumatic suspension with piezoelectric energy harvester," *Smart Materials and Structures*, vol. 32, no. 7, article 075005, 2023.

[22] Z. Zhao, B. F. Zhang, Y. X. Li, C. J. Bao, and T. Wang, "A novel piezoelectric energy harvester of noncontact magnetic force for a vehicle suspension system," *Energy Science & Engineering*, vol. 11, no. 3, pp. 1133–1147, 2022.

[23] C. F. Wei and X. J. Jing, "A comprehensive review on vibration energy harvesting: modelling and realization," *Renewable & Sustainable Energy Reviews*, vol. 74, pp. 1–18, 2017.

[24] M. Wang, Y. M. Xia, H. Y. Pu et al., "Piezoelectric energy harvesting from suspension structures with piezoelectric layers," *Sensors*, vol. 20, no. 13, p. 3755, 2020.

[25] Q. Zhao, Y. N. Liu, L. B. Wang, H. L. Yang, and D. W. Cao, "Design method for piezoelectric cantilever beam structure under low frequency condition," *International Journal of Pavement Research and Technology*, vol. 11, no. 2, pp. 153–159, 2018.

[26] L. L. Li, J. Xu, J. T. Liu, and F. Cao, "Recent progress on piezoelectric energy harvesting: structures and materials," *Advanced Composites and Hybrid Materials*, vol. 1, no. 3, pp. 478–505, 2018.

[27] B. Mahale, N. Kumar, A. De, R. Pandey, and R. Ranjan, "A comparative study of energy harvesting performance of polymer-piezoceramic composites fabricated with different piezoceramic constituents," *International Journal of Energy Research*, vol. 45, no. 2, pp. 2694–2708, 2021.

[28] J. P. Ma, K. Zhu, D. Huo et al., "Performance enhancement of 1-3 piezoelectric composite materials by alternating current polarising," *Ceramics International*, vol. 47, no. 13, pp. 18405–18410, 2021.

[29] D. S. Nguyen, E. Halvorsen, G. U. Jensen, and A. Vogl, "Fabrication and characterization of a wideband MEMS energy harvester utilizing nonlinear springs," *Journal of Micromechanics and Microengineering*, vol. 20, no. 12, article 125009, 2010.

[30] V. Meruane and K. Pichara, "A broadband vibration-based energy harvester using an array of piezoelectric beams connected by springs," *Shock and vibration*, vol. 2016, Article ID 9614842, 13 pages, 2016.

[31] H. Abramovich and I. Har-nes, "Analysis and experimental validation of a piezoelectric harvester with enhanced frequency bandwidth," *Materials*, vol. 11, no. 7, p. 1243, 2018.

[32] G. B. Hu, J. L. Wang, H. W. Qiao, L. Y. Zhao, Z. Y. Li, and L. H. Tang, "An experimental study of a two-degree-of-freedom galloping energy harvester," *International Journal of Energy Research*, vol. 45, no. 2, pp. 3365–3374, 2020.

[33] Y. Qin, S. Wang, T. T. Wei, and R. Chen, "A wide band nonlinear dual piezoelectric cantilever energy harvester coupled by origami," *Smart Materials and Structures*, vol. 30, no. 2, article 025025, 2021.

[34] M. Khalili, A. B. Biten, G. Vishwakarma, S. Ahmed, and A. T. Papagiannakis, "Electro-mechanical characterization of a piezoelectric energy harvester," *Applied Energy*, vol. 253, article 113585, 2019.

[35] E. H. A. Niasar, M. Dahmardeh, and H. S. Googarchin, "Roadway piezoelectric energy harvester design considering electrical and mechanical performances," *Proceedings of the Institution of Mechanical Engineers Part C-Journal of Mechanical Engineering Science*, vol. 234, no. 1, pp. 32–48, 2020.

[36] Y. Cao, F. Zhang, A. Sha, Z. Liu, Y. Hao, and Y. Hao, "Energy conversion models and characteristics under various inner connections of a novel packaged piezoelectric transducer for pavements," *Energy Conversion and Management*, vol. 245, article 114563, 2021.

[37] Y. Li, C. J. Xie, S. H. Quan, W. L. Li, and Y. Shi, "Maximization of piezoelectric vibration energy harvesting of vehicle based on double-gear drive," *Energy Science & Engineering*, vol. 7, no. 5, pp. 1948–1960, 2019.

[38] Y. Li, C. J. Xie, S. H. Quan, C. N. Zen, and W. L. Li, "Vibration energy harvesting in vehicles by gear segmentation and a virtual displacement filtering algorithm," *International Journal of Energy Research*, vol. 42, no. 4, pp. 1702–1713, 2018.

[39] J. G. Smits and W. S. Choi, "The constituent equations of piezoelectric heterogeneous bimorphs," *IEEE Transactions on Ultrasonics Ferroelectrics and Frequency Control*, vol. 38, no. 3, pp. 256–270, 1991.

[40] M. S. Weinberg, "Working equations for piezoelectric actuators and sensors," *Journal of Microelectromechanical Systems*, vol. 8, no. 4, pp. 529–533, 1999.